Regenerative Braking Energy Utilization Analysis in AC/DC Railway Power Supply System with Energy Feedback Systems

Jian Zhang, Zhongbei Tian, Wei Liu, Lin Jiang, Jiaxin Zeng, He Qi, and Yuheng Yang

***Abstract*—In the power supply system with energy feedback system (EFS)s, the energy from EFS (WF) will flow to rectifiers, which is circulation flow (CF). However, the efficiency of CF between substations has been rarely studied. Besides, the relationship between the train operation and regenerative braking energy (RBE) utilizing efficiency is not clear. In this paper, the energy flow structure of the AC/DC railway power supply system including CF is established. In the double-train system, promoting CF when the trains' distance is long can be beneficial to power utilization efficiency. Chengdu Metro Line 9 is analyzed as the multi-train system based on the iterative AC/DC power flow algorithm. The key to energy saving includes reducing the energy consumption of on-board resistance and the DC traction network loss. Compared with the catenary and rail system, the fourth-rail system can promote system energy efficiency by 23.5% at most. The CF and energy fed to main substations counts for less than 2% and 8% of WF. When the headway time is short, RBE should be avoided feedback to EFS, while the feedback power of EFS should be advocated when the headway time is long. The results can help guide the operation of urban rail to save energy.**

***Index Terms*—Regenerative Braking Energy; Circulation Flow; Energy feedback system (EFS); AC/DC power supply system**

NOMENCLATURE

Symbol/Abbreviation	Definition
MS	Main substation
TS	Traction substation
SS	Step-down substation
EFS	Energy feedback system
RBE	Regenerative braking energy
ETT	Energy transferred between trains
CF	Circulation flow
TN	Traction network
W_M	Active energy consumed by all MSs

This work was supported by the China Scholarship Council.

J. Zhang, W. Liu, J. Zeng, H. Qi, Q. Li are with School of Electrical Engineering, Southwest Jiaotong University, Chengdu, China (e-mail:,zhangjian95@foxmail.com, liuwei_8208@swjtu.cn, zjx9805@163.com, zy728734777@163.com, yyh838766021@my.swjtu.edu.cn).

Z. Tian, L. Jiang is with the Department of Electrical Engineering and Electronics, the University of Liverpool, Liverpool, U.K. (e-mail: Zhongbei.tian@liverpool.ac.uk, ljiang@liverpool.ac.uk).

(*Corresponding author: Zhongbei Tian, Wei Liu*)

W_T	Traction energy of TSs at DC side
W_F	Energy fed at the AC side by the EFSs
W_R	Energy fed to the MSs
W_S	Energy consumed by all SSs
W_{res}	Energy consumed by the on-board resistors
W_{trac}	Traction energy of all trains
W_{reg}	RBE of all trains
W_{ETT}	The ETT in the system
W_{CF}	Circulation flow energy
$W_{ConvLoss}$	The energy loss of rectification
$W_{InvLoss}$	The energy loss of inversion
W_{DCLoss}	The energy loss on the DC side
W_{k+aux}	The sum of kinetic energy and auxiliary energy
W_S	The energy of step-down loads
η_T	Efficiency of rectifiers
η_F	Efficiency of the EFSs
P_{Ti}	The power at the AC side of the TS
P_{Si}	The active power of *i*th substation's step-down load
$P_{train i}$	The power of the *i*th train
P_{Reci}	The power of the rectifier unit at the DC side in *i*th TS
P_{EFSi}	The power of EFS at the DC side in *i*th TS
$P_{ConvLoss}$	The power loss of rectification
$P_{InvLoss}$	The power loss of inversion
P_{DCLoss}	The power loss on the DC side

I. INTRODUCTION

In the power supply system of urban rail, there is great potential for RBE utilization because of the frequent braking of trains. Some devices, like the on-board resistor, consume the RBE in an unsustainable way, because they turn RBE into thermal energy. With the development of technology and the study of RBE utilization, EFS, energy storage system (ESS), and bidirectional converter device (BCD) are widely applied worldwide [1]-[3]. Other technologies include bypass DC Loop [4] and so on. With these devices, the RBE flow is more complicated than before. To utilize the devices better and improve system efficiency, deep research into RBE utilization is necessary. In this paper, only the urban rail system with EFSs is discussed.

EFS can feedback RBE to the AC side, and there are three whereabouts: step-down loads, main substation (MS)s, and rectifiers. The third one is called CF. The inhibition of CF inside the TS can be realized by promoting device design [4][5] and setting feasible parameters. The relevant research is mature. However, the CF between TSs is difficult to avoid. [7] points out that CF between TSs should be minimized. The energy transfer process through CF will cause losses in both the EFS and the rectifier, and therefore be inefficient in theory. But it has not been studied in depth. Quantified efficiency comparison of CF and ETT is indispensable for RBE utilization analysis.

Analyzing the energy flow structure is vital. In [8][9], the energy flow structure between trains is analyzed, but it only suits high-speed railways. In [10], the distribution of RBE is analyzed, but it does not consider the AC side. In [11], only the structure of energy flow between trains is analyzed, but the overall energy flow is not analyzed systematically. In [12]-[14], the energy flow structure including rectifiers is analyzed, but the EFSs are not considered. In [15], the energy flow path of the EFS is added, but the MSs and their related energy flow path are not taken into account. In [16] and [25], the energy flow structure is analyzed, but the

energy flow of trains is not continuous with the energy flow between trains. The CF is neglected. To analyze the energy flow, energy flow analysis in detail is needed.

The accurate analysis is based on the precise algorithm. However, rectifier and inverter devices are uniformly modeled without considering power reversal during inversion. In [17]-[20], train movement, electrical networks, and traction substations are modeled, but EFS is not considered. In [21] and [22], different types of traction substations are modeled, but the EFS model was not mentioned. In [23], a reasonable steady-state model for a voltage source converter is created, and an alternative algorithm of the AC/DC hybrid system power flow is proposed. But it does not suit the urban rail. In [24]-[26], AC/DC unified power flow calculation considering the constant power state of EFS is proposed. For AC/DC alternative power flow algorithm, the constant power state of EFS is rarely added into consideration.

Timetable optimization and energy-efficient driving are two mainly used train operation methods. The former method aims to maximum the utilization of RBE, and has been studied for a long time. The main differences in existing research are optimization objectives, models, and algorithms. Utilization of RBE is mainstream objective, while passenger travel time [27] and overlapping time [30] can also be objectives. As for the model, except for the integer programming model [31], there are other models, such as the energy-saving operation model for multiple trains considering different operation modes of the trains [28], multi-train trajectory optimization method is proposed to find optimal meeting locations, arrival/departure times, and speed trajectories [29], integrated model which includes both the timetable and the train trajectory [32]. For the algorithm, genetic algorithm (GA) is widely used [27][30][31]. And some modified algorithms are also effective, such as GA-PSO [32], parallelized particle swarm optimization based on Map-Reduce (PPSO-MR) [33] and so on. The above researches focus on optimization methods but do not clarify the relationship between timetable and RBE. [10] points out it is difficult to find explicitly mathematical relationships between timetable adjustment and utilization of RBE. To solve this problem, correlation analysis can be an effective approach.

The main contributions of this paper can be summarized as follows:

1) The traction power supply system energy flow structure considering CF is analyzed in detail. The key to the system traction energy saving includes reducing the on-board resistance energy consumption and DC loss energy consumption. The results of the theoretical analysis are verified by the simulation of the practical railway route, Chengdu line 9.

2) The power utilization efficiencies are compared when trains and EFS state are different in the static system. The existence of CF does not always reduce the efficiency of the system. On the contrary, the power utilization efficiency is higher than that of ETT when the trains' distance is long.

3) Through simulation, the advantage of the fourth-rail system in energy saving is quantified compared with the catenary and rail system, which can guide the decision of system design.

4) The energy flow component, energy efficiency, and correlation under different timetables of trains are analyzed. When

headway time is short, to save energy, RBE should be avoided feedback by EFSs, while ETT should be suppressed when the headway time is long. The rules can guide the operation institutions of urban rail such as the adjustment of running maps.

This paper is organized as follows: Section II first analyzes the energy flow in the power supply system in detail, which contains the CF. Then the power of CF is defined. A simplified case analysis shows why AC cable loss can be neglected. In section III, the double-train system model is first, which includes the AC equivalent circuit and four DC equivalent circuits. Then the brake train power and train distance are taken as parameters. The impact of trains, EFS, and step-down loads are analyzed in order. In section IV, the improved AC/DC iterative power flow algorithm is proposed. Then a subway case is studied. The components of RBE and energy fed by EFSs under different headway times are analyzed. Then the correlation between energy at MS and other energies is analyzed.

II. Energy Flow for AC/DC Railway Power Supply System

The energy flow can reflect the energy structure and distribution in the power supply system of urban rail. Studying the energy flow is necessary, for it helps schedule the train operation, and set reasonable parameters for EFSs to improve the efficiency of the system and save energy.

In the urban rail power supply system, the structure is shown in Fig. 1. The MSs transform AC 110kV to AC 35 kV and connect the AC 35 kV buses. The buses then connect to the TSs and SSs. In TSs, the rectifiers convert AC 35kV to DC 1500V and are connected to DC 1500V buses. The buses connect to the TN and the EFSs. EFSs can feed energy from the DC bus to AC 35 kV side. The step-down loads obtain energy from step-down transformers. In SSs, there are only step-down loads. The TN includes the feeder, up-down catenary, up-down rail, return conductor, etc.

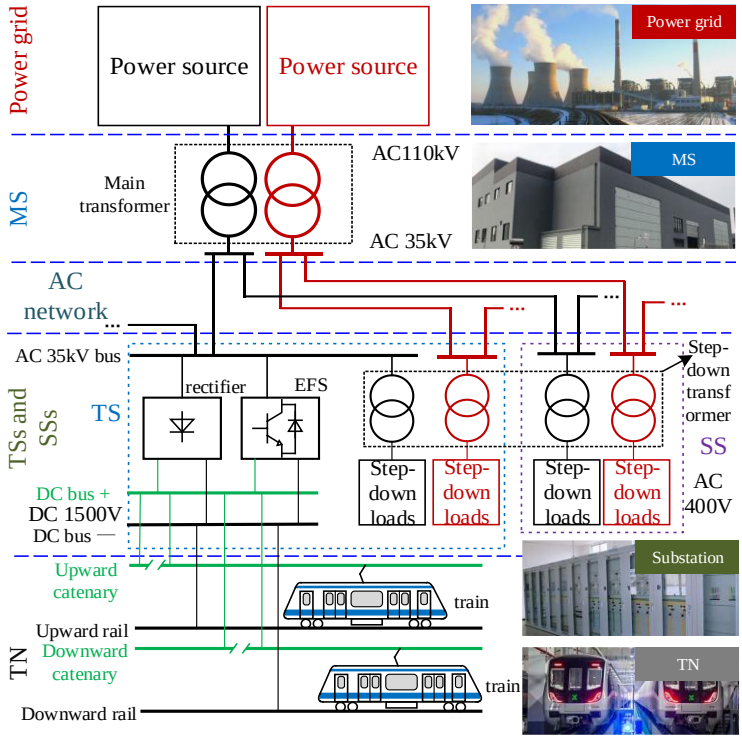

Fig. 1 The structure of the power supply system in urban rail

A. Energy Flow Structure

The energy flow structure is shown in Fig. 2. It is assumed that power losses on the AC cables are ignored. The power starts from MSs as W_M. In the AC network, W_M flows to TSs and SSs. The receivers are rectifiers and step-down loads. For rectifiers, they provide traction energy for trains (W_{trac}), but the process has energy losses on rectifiers and the TN, which are $W_{ConvLoss}$ and W_{DCLoss}. The traction energy will become kinetic energy and auxiliary energy (W_{k+aux}), traction loss ($W_{TracLoss}$), and RBE (W_{reg}). There are three main whereabouts for RBE: consumed on on-board resistors (W_{res}), ETT (W_{ETT}), and fed back by EFS. The power loss through EFSs is $W_{InvLoss}$. The energy fed to the AC side (W_F) also has three whereabouts: CF(W_{CF}), fed to MSs (W_R), and consumed by step-down loads. For W_{reg}, it has two paths to flow back to traction trains: ETT and CF. The paths are shown in Fig. 2.

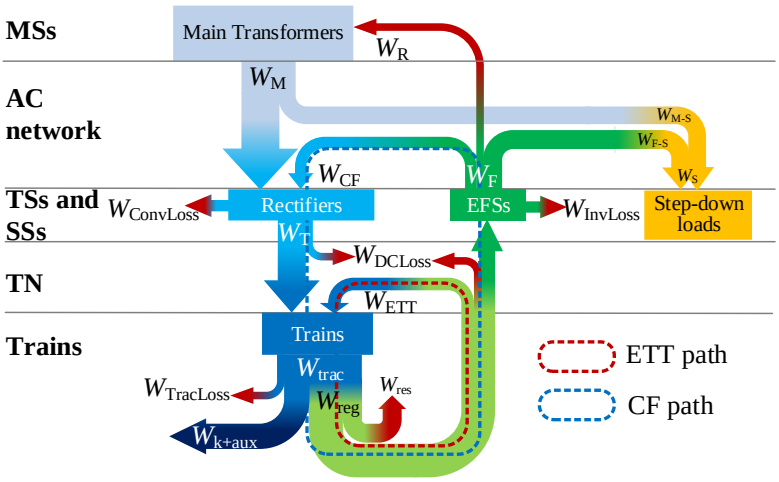

Fig. 2 The energy flow diagram

According to [34], the power supply system without EFSs is defined as the reference system (RS). The power supply system with EFS installed is defined as the contradistinction system (CS). The superscript " ′ " means the parameter in RS. The energy functions can be obtained as:

$$\begin{cases} W_M = W_T / \eta_T + W_S - W_F + W_R \\ W_M{}' = W_T{}' / \eta_T + W_S \\ W_T = W_{k+aux} + W_{TracLoss} + W_{res} + W_{DCLoss} + W_F / \eta_F \\ W_T{}' = W_{k+aux} + W_{TracLoss} + W_{res}{}' + W_{DCLoss}{}' \end{cases} \tag{1}$$

And the system-level energy consumption (STEC) index is defined as:

$$\begin{cases} W_{TR} = W_T / \eta_T - W_F + W_R \\ W_{TR}{}' = W_T{}' / \eta_T \end{cases} \tag{2}$$

Therefore, the energy difference between the two systems is energy saving. It is as (3). Since the coefficient of W_F is near 0, it can be seen that the key to the system traction energy saving includes reducing the energy consumption of on-board resistance, the loss of DC TN, and the energy fed to MSs.

$$W_{TR}{}' - W_{TR} = W_{res}{}' - W_{res} + W_{DCLoss}{}' - W_{DCLoss} + \frac{\eta_T \eta_F - 1}{\eta_F} W_F - \eta_T W_R \tag{3}$$

B. Definition of CF between TSs

It is worth mentioning that there are mainly two kinds of CF: the CF in the TS and the CF between TSs. The former is not preferable for the efficient operation of urban rail, but it can be eradicated by improving the control method of converters. The latter is what is discussed in this paper.

The structure diagram of one bus in a power supply section is shown in Fig. 3. The TSs are connected to MS through cables. For a TS, there are two lines out. The line which is from the MS is called the incoming line, and the other is the outcoming line. The CF can be sequential CF (SCF) or reverse CF (RCF). For the RCF, the energy fed back by the EFS will be passed to the TSs which are closer to MS in topology. For the SCF, the energy fed back by the EFS will be passed to the TSs which are farther from MS in topology.

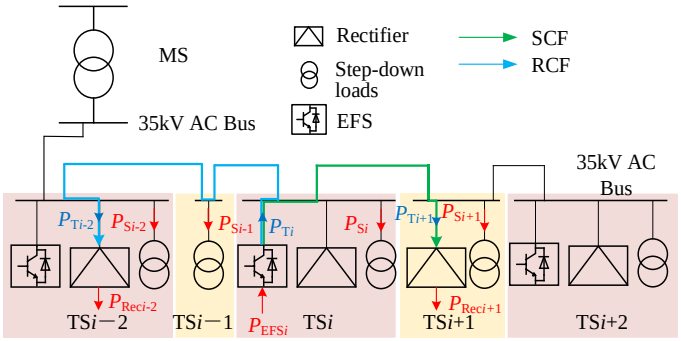

Fig. 3 Structure of CF in a power supply section

The CF only exists when the rectifier and EFS work simultaneously in the power supply section.

$$\begin{cases} P_{\mathrm{T}i} = \eta_{\mathrm{F}} P_{\mathrm{EFS}i} \\ P_{\mathrm{Rec}n} = \eta_{\mathrm{T}} P_{\mathrm{T}n} \end{cases} \tag{4}$$

It is assumed that the feedback energy will first flow to sequential TSs and SSs. The SCF power of TSi, $P_{\mathrm{SCF}i}$, should be calculated first. If the EFS of TSi is working, the P_{SCF} is as (5). In which, (i+j1), (i+ j2),⋯ are the numbers of TSs that have rectifiers in operation and farther from MS than TSi in topology. Especially, when TSi is at the end of the power supply section, the SCF power is 0.

$$P_{\mathrm{SCF}i} = \begin{cases} 0 & P_i < \sum_{n=0}^{j1} P_{\mathrm{S}i+n} \\ \eta_{\mathrm{T}}(P_i - \sum_{n=0}^{j1} P_{\mathrm{S}i+n}) & \sum_{n=0}^{j1} P_{\mathrm{S}i+n} \le P_i < (\sum_{n=0}^{j1} P_{\mathrm{S}i+n} + P_{i+j1}) \\ P_{\mathrm{Rec}i+j1} & (\sum_{n=0}^{j1} P_{\mathrm{S}i+n} + P_{i+j1}) \le P_i < (\sum_{n=0}^{j2} P_{\mathrm{S}i+n} + P_{i+j2}) \\ \cdots \end{cases} \tag{5}$$

Then calculate RCF part and $P_{\mathrm{CF}i}$ can be obtained. In which, (i-k1), (i-k2),⋯ are the numbers of TSs which have rectifiers in operation and are closer to MS than TSi in topology.

$$P_{\mathrm{CF}i} = \begin{cases} P_{\mathrm{SCF}i} & P_i < (P_{i+} + \sum_{n=0}^{k1} P_{\mathrm{S}i-n}) \\ P_{\mathrm{SCF}i} + \eta_{\mathrm{T}}(P_{\mathrm{EFS}i} - P_{i+} - \sum_{n=0}^{k1} P_{\mathrm{S}i-n}) & (P_{i+} + \sum_{n=0}^{k1} P_{\mathrm{S}i-n}) \le P_i < (P_{i+} + \sum_{n=0}^{k1} P_{\mathrm{S}i-n} + P_{i-k1}) \\ P_{\mathrm{SCF}i} + P_{\mathrm{Rec}i-k1} & (P_{i+} + \sum_{n=0}^{k1} P_{\mathrm{S}i-n} + P_{i-k1}) \le P_i < (P_{i+} + \sum_{n=0}^{k2} P_{\mathrm{S}i-n} + P_{i-k2}) \\ \cdots \end{cases} \tag{6}$$

Where P_{i+} is the traction and step-down loads of substations that are farther from MS than TSi in topology. N is the number of substations in the power supply section. (i+J) is the farthest TS from MS in topology which has the working rectifier.

$$P_{i+} = \sum_{n=0}^{N-i} P_{\mathrm{S}i+n} + \sum_{n=j1}^{J} P_{\mathrm{Rec}i+n} \tag{7}$$

The total CF, P_{CF} is as (8). The step-down loads should be calculated only once. They should be calculated by the nearest EFS if there are more than one EFS that can provide energy for the step-down load.

$$P_{CF} = \sum_{i=1}^{N} P_{\mathrm{CF}i} \tag{8}$$

C. Analysis of Losses by Circulation Flow

To analyze the loss through the CF path, a simplified case is established with the following assumed conditions are:

- There are 2 TSs and 2 trains.
- The path of CF is train1→EFS in TS1→AC cable→rectifier unit in TS2→train2.
- There is no power supplied to TS2 from the power grid.
- The impedance between the regenerative braking train and EFS and the impedance between the rectifier unit and traction train are ignored.
- The distance between two TSs is 3 km.

R and x are the impedance per unit length of the AC side cable. b is the susceptance per unit length of the AC side cable. The parameter values are shown in Table I. P_{S1} and P_{S2} in this case are both 240kW. $P_{\mathrm{ACCableLoss}}$ is the power loss on AC cable. P_{InvLoss} and P_{ConvLoss} are calculated as (9).

$$\begin{cases} P_{\mathrm{Invloss}} = (1-\eta_{\mathrm{F}})P_{\mathrm{EFS2}} \\ P_{\mathrm{Convloss}} = (1-\eta_{\mathrm{T}})P_{\mathrm{T1}} \end{cases} \tag{9}$$

TABLE I SOME PARAMETER VALUES

Parameter	Value	Parameter	Value
R/(Ω/km)	0.0529	x/(Ω/km)	0.045
b/(S/km)	0.141×10^{-3}	η_{Rec}	0.98
η_{EFS}	0.95		

P_{EFS1} is the power of EFS in TS1. The power losses are shown in Fig. 4. When P_{EFS1} is 8MW, the sum of P_{InvLoss} and P_{ConvLoss} is 567kW, while $P_{\mathrm{ACCableLoss}}$ loss is only 1.5kW. As the current is small at the 35kV side, the AC cable loss can be ignored, and the main loss occurs in the power commutation process of the converters.

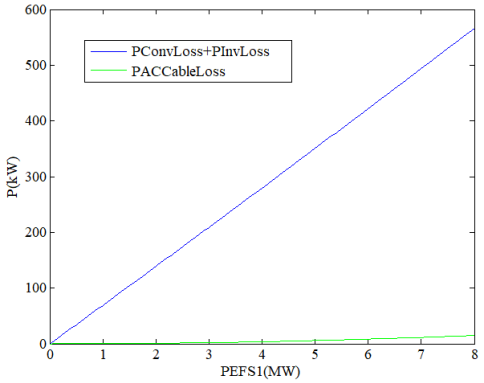

Fig. 4 The P_{EFS1} and power losses

III. Energy Transfer Comparison in Static System

A double-train model is built for analyzing the energy flow and comparing two energy transfer ways. It is shown in Fig 2. There are two TSs. TS1 connects to the outcoming line of the MS after passing through several TSs and SSs. TS2 is at the end of the power supply partition of the MS. Train1 is in traction mode; train2 is in regenerative braking mode. The analysis in this chapter is for a specific moment, so it is a static system.

If P_{T1} and P_{T2} are both positive, CF between TSs exists. The CF path and the ETT path are shown in Fig. 5. After satisfying the train1 and step-down loads of TS1 and TS2, the redundant CF power will flow to other step-down loads. This part of the energy is P_{Other}. Assume that P_{Other} is fully utilized, and the loss is ignored.

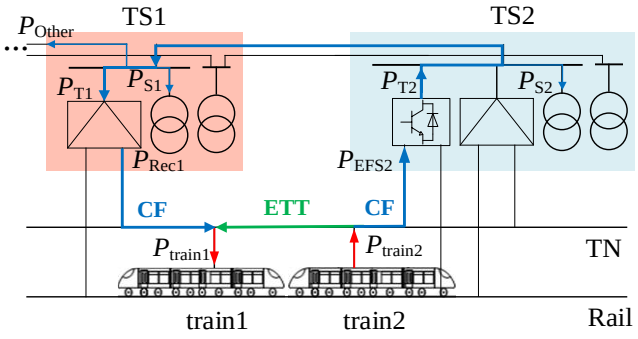

Fig. 5 Schematic diagram of the double-train system

A. *Modeling Double-train System*

In the double-train model, the rectifier and EFS may not work due to the fluctuation of the TN's voltage. Therefore, there are four equivalent DC circuits, as shown in Fig. 7. Four Cases are defined. The AC equivalent circuit is shown in Fig. 6. U_0 is the no-load voltage of the rectifier. R_0 is the equivalent inner resistance of the rectifier.

In Case A to Case C, at least one converter works. The trains are built as power sources. The power of train1 and train2 are P_{train1} and P_{train2} in Case A to Case C. In Case D, train1 is built as a voltage source, so the circuit has reasonable solutions. Its voltage is U_{train2}.

The unit length resistance of TN is r. The distance between TS1 and TS2 is L. l_1 is the distance between train1 and TS2. l_2 is the distance between train2 and TS2. U_1~U_4 are the voltages of nodes. I_1~I_4 are currents. I_{EFS} and I_{Rec} are the currents of the EFS and rectifier.

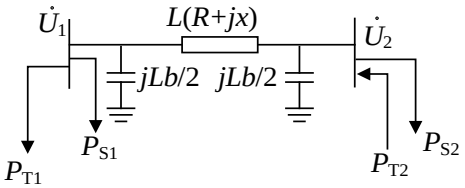

Fig. 6 The equivalent AC circuit diagram of the double-train model

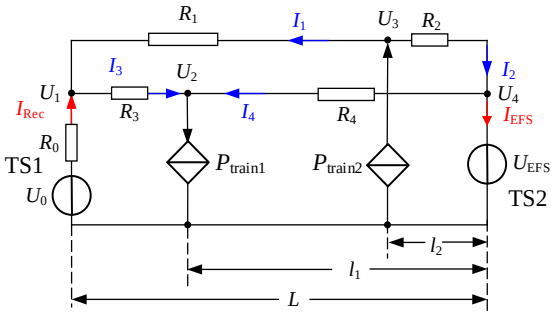

Case A

(a)

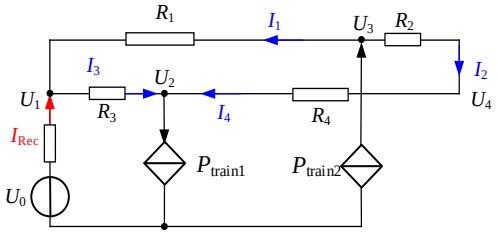

Case B

(b)

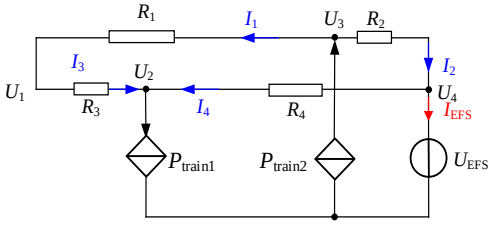

Case C

(c)

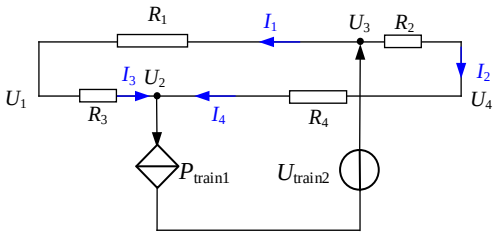

Case D

(d)

Fig. 7 The equivalent DC circuit diagram of the double-train model

(a)Case A: Both EFS and rectifier work; (b)Case B: Rectifier works and EFS does not work; (c)Case C: the EFS works and rectifier does not work. (d)Case D: EFS and rectifier neither work.

The node voltage method is applied to solve circuits in Case A to Case C. The equations are (10). G_0~ G_4 are the reciprocal of R_0~ R_4 and the corresponding conductance. P_{CF} is as (11).

$$\begin{cases} (G_0+G_1+G_3)U_1-G_3U_2-G_1U_3=U_0/R_0 \\ (G_3+G_4)U_2-G_3U_1-G_4U_4=-P_{\text{train1}}/U_2 \\ (G_1+G_2)U_3-G_1U_1-G_2U_4=P_{\text{train2}}/U_3 \end{cases} \quad \text{Case A}$$

$$\begin{cases} (G_0+G_1+G_3)U_1-G_3U_2-G_1U_3=U_0/R_0 \\ (G_3+G_2\,\|\,G_4)U_2-G_3U_1-(G_2\,\|\,G_4)U_3=-P_{\text{train1}}/U_2 \\ (G_1+G_2\,\|\,G_4)U_3-G_1U_1-(G_2\,\|\,G_4)U_2=P_{\text{train2}}/U_3 \end{cases} \quad \text{Case B} \qquad (10)$$

$$\begin{cases} (G_1\,\|\,G_3+G_4)U_2-(G_1\,\|\,G_3)U_3-G_4U_4=-P_{\text{train1}}/U_2 \\ (G_1\,\|\,G_3+G_2)U_3-(G_1\,\|\,G_3)U_2-G_2U_4=P_{\text{train2}}/U_3 \end{cases} \quad \text{Case C}$$

$$P_{CF}=\begin{cases} P_{\text{Rec1}} & \text{if } P_{\text{Rec1}}<\eta_T(P_{T2}-P_{S1}-P_{S2}) \quad \text{in CaseA} \\ \eta_T(P_{T2}-P_{S1}-P_{S2}) & \text{if } 0<\eta_T(P_{T2}-P_{S1}-P_{S2})\le P_{\text{Rec1}} \quad \text{in CaseA} \\ 0 & \text{other cases} \end{cases} \qquad (11)$$

Since there are four cases in Fig. 7, a calculation algorithm is needed to judge which one is suitable. The algorithm is based on Case A, which contains both the rectifier and EFS. After the first calculation of the double-train model, the current of rectifier and EFS can be obtained. State adjustment can take the current as the criterion. Then the updated model is applied to calculate the results. The calculation process is shown in Fig. 8. First, the simulation parameters of the double-train model are input. Then the Case A model is solved. In the results, I_{EFS} and I_{Rec} are obtained. If they are both not negative, then the results can be output. If I_{EFS} is not negative and I_{Rec} is negative, the Case B model should be applied to calculate again. If I_{EFS} is negative and I_{Rec} is not negative, the Case C model should be applied to calculate again. If they are both negative, the Case D model should be applied to calculate again.

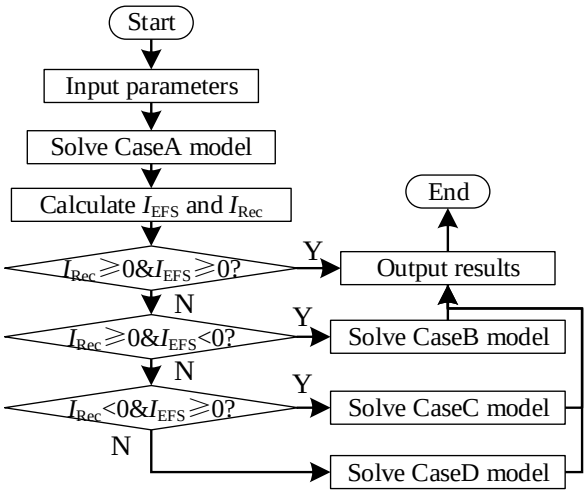

Fig. 8 Calculation Process of Case A

B. The Power Flow and Power Utilization Efficiency

Fig. 9 shows the power flow diagram of the double-train model. The power sources are the train2 and the power net, which means power from the MS. The power from the power net is P_{Net}. The power receivers are the train1, the step-down loads of TS1 and TS2, and other step-down loads. There are two power flow paths from P_{train2} to P_{train1}: ETT and CF, which correspond to two paths in Fig. 5. P_{Loss} is the total loss when transferring energy. Since the model is complicated, some power paths may be zero in some specific cases.

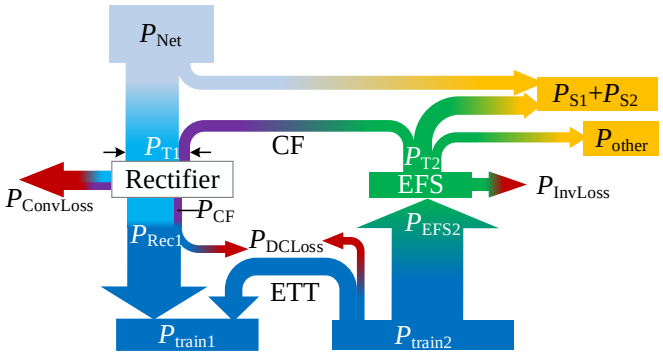

Fig. 9 The power flow diagram of the double-train model

The power utilizing efficiency, η_P is defined as the power of loads to the power of sources. P_{Load} is the power of loads. P_{Source} is the power of sources. η_P is as (12). It is assumed that if P_{CF} is greater than P_{T1}, the redundant power can be utilized by other step-down loads in other TSs.

$$\eta_P = \frac{P_{Load}}{P_{Source}} = \frac{P_{train1}+P_{S1}+P_{S2}+P_{Other}}{P_{train2}+P_{Net}} = \frac{P_{Load}}{P_{Load}+P_{Loss}} \tag{12}$$

where P_{Net}, P_{Other} and P_{Loss} are:

$$
\begin{aligned}
P_{\text{Net}} &= \begin{cases}
\begin{cases} 0 & \text{if } P_{\text{CF}} = P_{\text{Rec1}} \\ P_{\text{T1}} - P_{\text{CF}}/\eta_{\text{T}} & \text{if } P_{\text{CF}} = \eta_{\text{T}}(P_{\text{T2}} - P_{\text{S1}} - P_{\text{S2}}) \\ P_{\text{T1}} - P_{\text{T2}} + P_{\text{S1}} + P_{\text{S2}} & \text{if } P_{\text{CF}} = 0 \end{cases} & \text{Case A} \\
P_{\text{T1}} + P_{\text{S1}} + P_{\text{S2}} & \text{Case B} \\
\begin{cases} P_{\text{S1}} + P_{\text{S2}} - P_{\text{T2}} & \text{if } P_{\text{T2}} \le (P_{\text{S1}} + P_{\text{S2}}) \\ 0 & \text{if } P_{\text{T2}} > (P_{\text{S1}} + P_{\text{S2}}) \end{cases} & \text{Case C} \\
P_{\text{S1}} + P_{\text{S2}} & \text{Case D}
\end{cases} \\
P_{\text{other}} &= \begin{cases} P_{\text{T2}} - P_{\text{S1}} - P_{\text{S2}} - P_{\text{CF}}/\eta_{\text{T}} & \text{if } P_{\text{CF}} = P_{\text{Rec1}} \text{ in Case A} \\ & \text{or } P_{\text{T2}} > (P_{\text{S1}} + P_{\text{S2}}) \text{ in Case C} \\ 0 & \text{other cases} \end{cases} \\
P_{\text{Loss}} &= P_{\text{InvLoss}} + P_{\text{ConvLoss}} + P_{\text{DCLoss}}
\end{aligned} \tag{13}
$$

C. *Result Analysis*

To analyze the double-train model, different cases are defined in Table II. In Table II, the "On" state of EFS means EFS is in operation, but it will not work if the TN voltage is lower than its start voltage. The "Off" state means EFS is turned off and will not work in any case. The simulation parameters of the double-train model are shown in Table III. l_2 and P_{train2} are set as variable parameters.

TABLE II CASES DEFINITION

Case	EFS	P_{train1}	$P_{\text{S}i}$
1	On	7MW	240kW
2	On	6MW	240kW
3	Off	7MW	240kW
4	On	7MW	120kW

TABLE III SIMULATION PARAMETERS

Parameter	Value	Parameter	Value
l_1	0.2km	L	3 km
R_0	0.05Ω	U_{EFS}	1720V
U_{train2}	1800V	r	0.0373Ω/ km

1) *Impact of Trains*

In Case 1, l_2 and P_{train2} are variable. The difference between Case 1 and Case 2 is the P_{train1}.

The P_{CF} of Case 1 and Case 2 are shown in Fig. 10. The P_{CF} is closely related to P_{EFS2} and P_{Rec1}. They are shown in Fig. 11.

In Case 1, P_{CF} exists when P_{train2} is greater than 7.5MW and l_2 is greater than 1km. When P_{train2} rises from 7.5MW to 9MW, P_{CF} first rises and then reduces. The reason for reducing is that P_{CF} is equal to P_{Rec1} according to (7). Fig. 11 shows that P_{Rec1} decreases. When l_2 increases, P_{CF} also increases. The reason is that with the increasing of l_2, the resistance between two trains increases, which blocks ETT and promotes CF.

In Case 2, the peak of P_{CF} is less than the peak of P_{CF} in Case1. That is because the traction power need of train1 of Case2 is less than the need in Case1. The variation trend of P_{CF} with l_2 and P_{train2} is the same as the trend in Case 1.

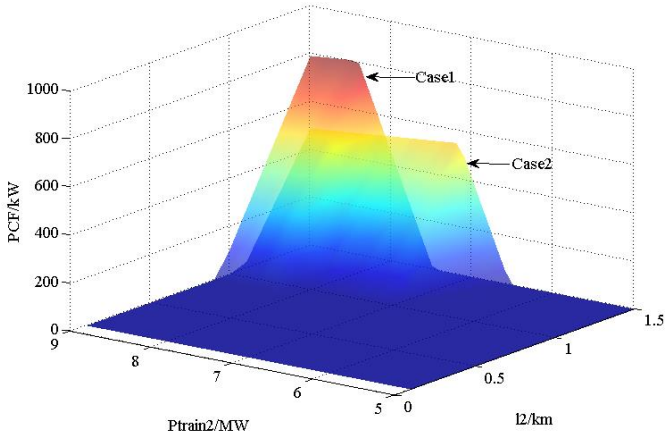

Fig. 10 P_{CF} of Case 1 and Case 2

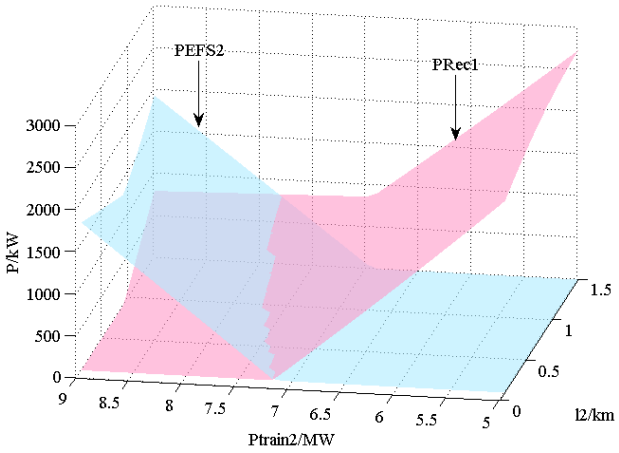

Fig. 11 P_{EFS2} and P_{Rec1} of Case 2.

The η_P of Case 1 and Case 2 is shown in Fig. 12. The closer the two trains are, the higher the η_P is, for the shorter power transmission length means less power loss in the process.

Generally speaking, η_P decreases as P_{train2} rises in Case1. But there is a rise when P_{train2} changes from 8.5MW to 9MW. The power of these two points is shown in Table IV. When P_{train2} rises from 8.5MW to 9MW, P_{Other} increases by 0.46MW. P_{CF} decreases by 0.01MW. Therefore, although P_{Loss} rises, the η_P still increases. The influence of P_{Other} is great to η_P in this section.

The η_P of Case 2 is higher than the η of Case 1 for most situations. The P_{Load} decreases and transmitted power between trains is less. Therefore, the η_P rises. However, when the P_{train2} is between 7MW and 9MW, and l_2 is between 0 and 0.5km, η_P of Case 2 is lower than the η_P of Case 1. This is also because of the influence of P_{Other}. In this situation, the equivalent circuit is Case C. The rectifier does not work, and P_{Other} is not 0. The P_{Other} of Case 1 is greater than the P_{Other} of Case 2, which means that there is more redundant W_F utilized by other step-down loads. It improves the η_P.

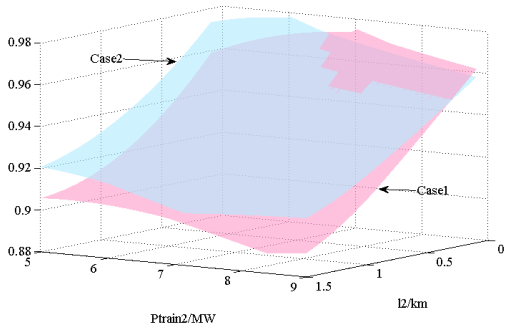

Fig. 12 η_P of Case 1 and Case 2

Table IV Power of two points in Case 1

P_{train1}/MW	7	7
P_{train2}/MW	8.5	9
P_{DCLoss}/MW	0.85	0.87
$P_{InvLoss}$+$P_{ConvLoss}$/MW	0.09	0.11
P_{Loss}/MW	0.94	0.98
P_{other}/MW	0.08	0.54
P_{CF}/MW	0.80	0.79
P_{Net}/MW	0	0
η_P	0.890	0.891

2) Impact of EFS

In Case 3, the EFS is off. The calculating process is as Fig. 13. First, the simulation parameters of the double-train model are input. Then the Case B model is solved. I_{Rec} can be obtained in the results. If it is no less than 0, the results can be output, or else the Case D model is applied and the calculation results are output. Case 1 and Case 3 have the same P_{Load}.

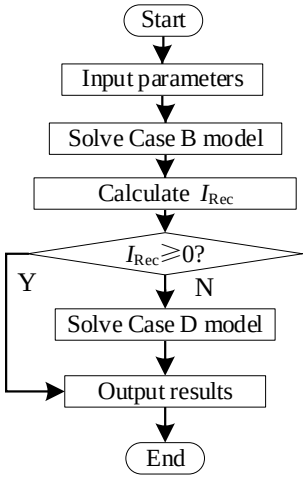

Fig. 13 Calculate process of Case 3

The η, P_{Loss}, and P_{DCLoss} of Case 1 and Case 3 are shown in Fig. 14, Fig. 15, and Fig. 16. To show the difference between Case 1 and Case 3 more clearly, the same data for Case 1 and Case 3 are not presented in Fig. 14 to Fig. 16.

In Case 1, EFS works. Therefore, some energy is transmitted through the AC side, which is P_{CF}. The energy transmitted on the DC side in Case 1 is less than the energy transmitted on the DC side in Case 3. So, P_{DCLoss} in Case 1 is less than P_{DCLoss} in Case 3,

as shown in Fig. 14. Meanwhile, P_{InvLoss}+P_{ConvLoss} in Case 1 is greater than P_{InvLoss}+P_{ConvLoss} in Case 3. According to (9), P_{Loss} consists of P_{DCLoss}, P_{InvLoss}, and P_{ConvLoss}. When l_2 is more than about 0.5km and P_{train2} is greater than 8MW, the difference of P_{DCLoss} is greater than the difference of P_{InvLoss}+P_{ConvLoss} between Case 1 and Case 3. Therefore, The P_{Loss} in Case 1 is less than the P_{Loss} in Case 3 in Fig. 15. The η_{P} of Case 1 is higher than the η_{P} of Case 3 in Fig. 16.

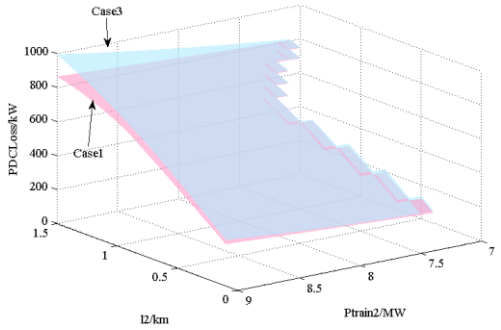

Fig. 14 P_{DCLoss} of Case 1 and Case 3

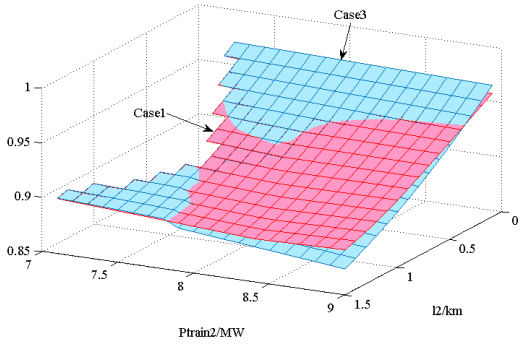

Fig. 15 η_{P} of Case 1 and Case 3

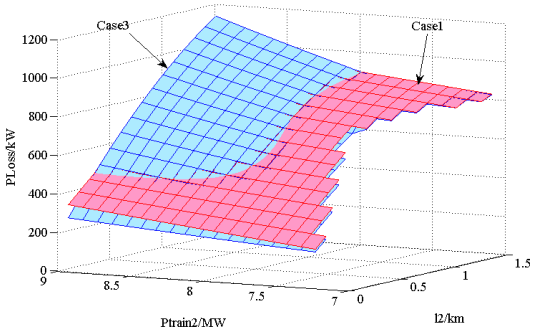

Fig. 16 P_{Loss} of Case 1 and Case 3

IV. Energy Analysis in Multi-train Dynamic System

A. Modeling of the Multi-train system and Solving Algorithm

The analysis in this chapter is for some time rather than a moment, so it is a dynamic system. The modeling of the multi-train system in urban rail mainly includes the TSs, TN, and trains. In this paper, the three-layer grounding network model of catenary,

rail, and ground is built. The rectifier unit is modeled as an ideal voltage source and a resistance in series by Thevenin equivalent circuit.

In the traditional AC/DC iterative power flow calculation algorithm, there are three states for TS: rectifying state (S_{Rec}), turn-off state (S_{Off}), and constant voltage state (S_{EFSU}). According to the output characteristic of EFS, it should have two working states: constant voltage state (S_{EFSU}) and constant power state (S_{EFSP}). When in S_{EFSU}, the EFS adopts the ideal voltage source model; When in S_{EFSP}, the EFS adopts the ideal power source model. The state transition is shown in Fig. 17(b). The judge conditions between S_{EFSP} and other states are:

- S_{EFSP} to S_{EFSU}: The voltage is lower than U_{EFS}.
- S_{EFSP} to S_{Off}: The current of EFS is lower than 0.
- S_{EFSU} to S_{EFSP}: The power of EFS is not lower than its rated power.

To improve the accuracy of calculation, the power source model is used to model the train in this paper. Besides, on-board resistance is also considered in the algorithm. After cutting the regenerative braking energy of trains, the reduced energy is calculated as the energy consumed by the on-board resistor. The calculation algorithm flow of the AC / DC power supply is shown in Fig. 17 (a). First, the parameters of the multi-train model are input. Then DC power flow is calculated until DC voltage converges. If the voltage of any train surpasses U_{on} (start voltage of on-board resistance) the RBE will be cut, and jump to DC power flow. Then judge the states of TSs. If there are unreasonable states, they will be updated, and jump to DC power flow. After that, AC power flow calculation will be implemented. If AC parameters converge, the calculation ends, or the process will come to DC power flow again.

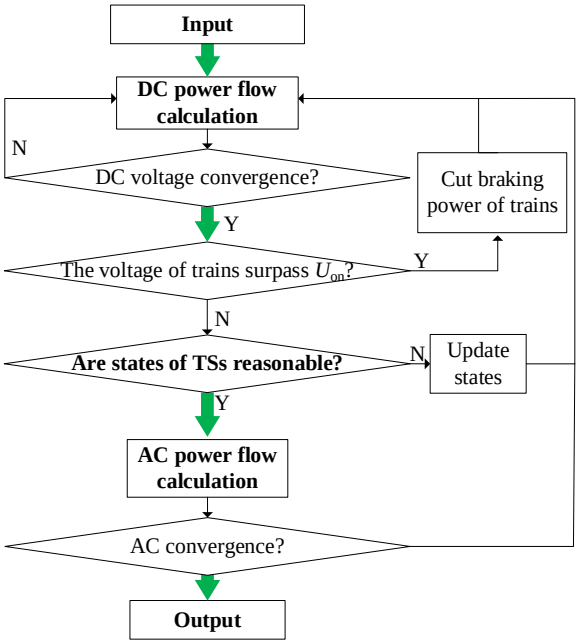

(a)

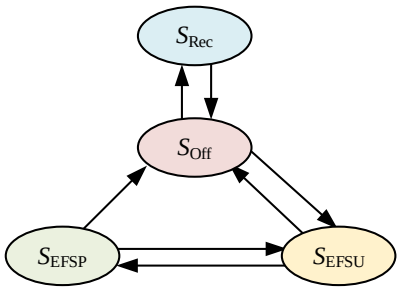

(b)

Fig. 17 The calculation algorithm of AC/DC power flow

(a) Algorithm process (b) State transition

B. Practical Line Modeling Data

Chengdu Metro Line 9 is studied. It has 2 MSs and 13 stations, including 11 TSs and 2 SSs. Its length is 40.45 km. The installation capacities of the main transformers are 2×40 MVA and 2×63 MVA. The rated power of the rectifier units is 2×3600 kW, and the no-load voltage is 1664 V. EFSs are installed at every other traction substation. The trains are 8As marshaling, with a top speed of 100 km/h, and the weight of 462 t. The structure is shown in Fig. 18, and the locations of each traction substation are shown in Table V. The catenary resistance is 0.0173 Ω/km, and the rail resistance is 0.02 Ω/km. The auxiliary power of trains is 300kW.

TABLE V LOCATION DISTRIBUTION OF TRACTION SUBSTATIONS OF CHENGDU METRO LINE 9

Traction substation	Location/km	Traction substation	Location/km
1	2.4	7	15.0
2	4.4	8	17.8
3	5.9	9	19.4
4	8.5	10	22.1
5	10.2	11	24.0
6	13.3		

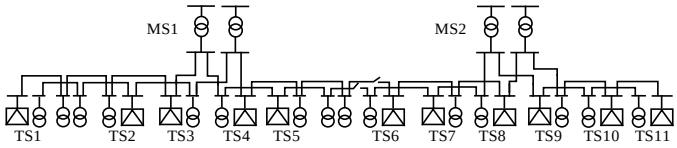

Fig. 18 The structure of Chengdu Metro 9

The headway time of trains is set as 150 s, 180 s, 200 s, 225 s, 300 s, 360 s, 450 s, and 600 s. To study the influence of different operation schedules, for each headway time, five operation schedules are set, which means the departure time difference between upward trains and downward trains. For example, when the headway time is 150s, the departure time difference between upward trains and downward trains is 0 s, 30 s, 60 s, 90 s, and 120 s.

All simulations were run using a personal computer with an Intel(R) Core (TM) i9-9900K CPU @ 3.60 GHz and 12 GB of RAM. The calculation time is shown in Table VI.

TABLE VI THE CALCULATION TIME UNDER DIFFERENT HEADWAY TIMES

Headway time(s)	120	180	240	300	400	450	600
Average iteration time(s)	323	309	346	314	388	391	410

C. *Energy Flow Component Analysis*

The energy results are shown in Table VII. The values are the average values of five operation schedules, and they are energy consumption per hour.

TABLE VII ENERGY RESULTS(KWH)

Headway time(s)	W_T/η_T	W_F	W_{trac}	W_{reg}	W_{res}	W_R	W_{CF}
150	17494	3754	24905	16422	1808	167	53
180	14351	3295	20759	13357	1145	160	66
200	12977	2688	18725	12416	1394	35	59
225	12394	3142	16639	11035	1260	67	43
300	9633	2525	12503	8432	1093	76	39
360	8305	2409	10417	7002	873	184	32
450	7008	2151	8333	5725	824	53	37
600	6568	1255	4404	2254	3964	943	14

To understand the relationship between RBE and the train operation timetable, the components of W_{reg} under different headway times are analyzed. The results are shown in Fig. 19. $W_{F\text{-}S}$ is the energy transmitted from EFSs to step-down loads. Among them, when W_{reg} flows to W_F and trains, the losses on TN are difficult to calculate separately, so this part of W_{DCLoss} is included in the calculation of the W_{ETT} ratio.

In Fig. 19, when the headway time increases, due to fewer trains, W_{reg} decreases. The distance between trains increases, which causes the decrease in the energy transfer between trains but promotes the percentage of W_F. The percentage of W_{res} in W_{reg} rises obviously when headway time increases from 450s to 600s. When headway time is great, the braking power of trains may overwhelm the capacity of EFSs, which increases the W_{res}.

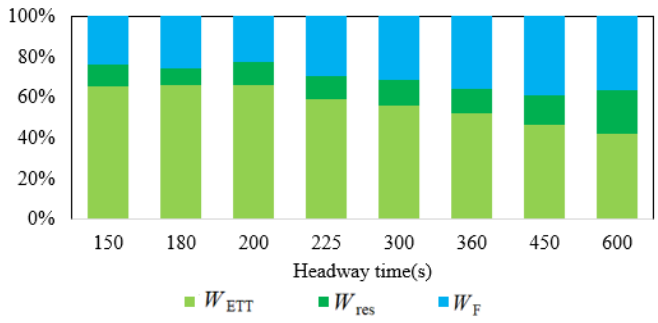

Fig. 19 The component analysis of W_{reg}

The components of W_F under different headway times are analyzed. The results are shown in Fig. 20. Although the percentage of W_F in W_{reg} increases, W_F decreases with the rise of headway time. The W_{CF} counts for less than 2% of W_F. The W_R counts for less than 8% of W_F. It indicates that in the multi-train system, the potential of promoting system efficiency by focusing on CF and energy fed to MSs is little.

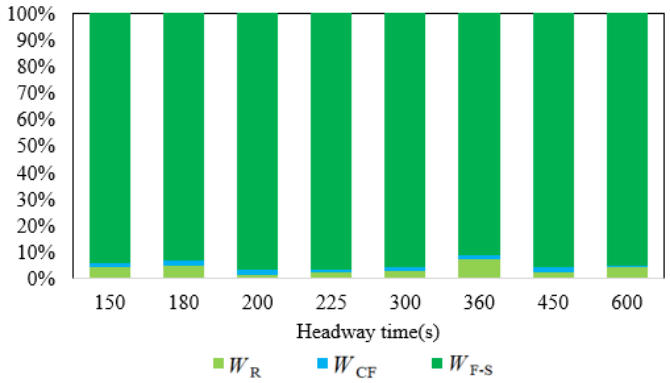

Fig. 20 The component analysis of W_F

D. Energy Efficiency Analysis

To study the influence of TN resistance on the system energy efficiency, the different cases are defined in Table VIII. Case 5 represents the catenary and rail system, which is the mainstream scheme. The parameters are introduced in section IV B. Case 6 fits the third-rail system. Case 7 fits the fourth-rail system. Other parameters of Case 6 and Case 7 are the same as the parameters of Case 5.

TABLE VIII CASES DEFINITION

Case	Positive TN	Negative TN	r
5	catenary	running rails	0.0373 Ω/km
6	conductor rail	running rails	0.0253 Ω/km
7	conductor rail	conductor rail	0.0160 Ω/km

From Fig. 2, the final receiver of traction energy is the kinetic energy and auxiliary energy of trains. Other energy is just intermediate quantities. Therefore, define the system energy utilizing efficiency, η_W as

$$\eta_W = \frac{W_{k+aux}}{W_{TR}} \tag{14}$$

The r can influence the system energy consumption. When studying the influence of r, the DC loss is of great importance. Define γ_{DCLoss} as the ratio of W_{DCLoss} to W_{trac}. It is shown in (15).

$$\gamma_{DCLoss} = \frac{W_{DCLoss}}{W_{trac}} = \frac{W_T + W_{reg} - W_{res} - W_{trac} - W_F/\eta_F}{W_{trac}} \tag{15}$$

The analysis results are shown in Fig. 22 to Fig. 24.

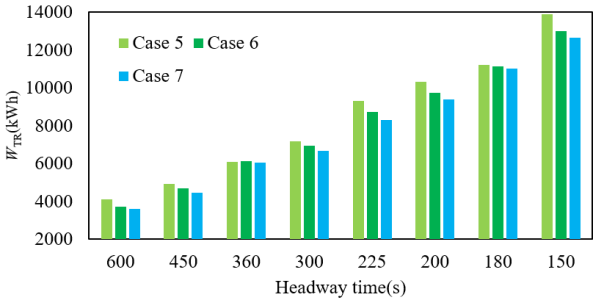

Fig. 22 The W_{TR} of different headway times

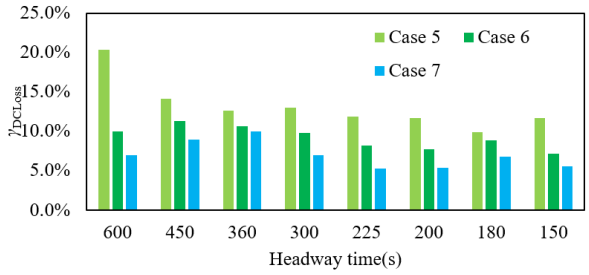

Fig. 23 The γ_{DCLoss} of different headway times

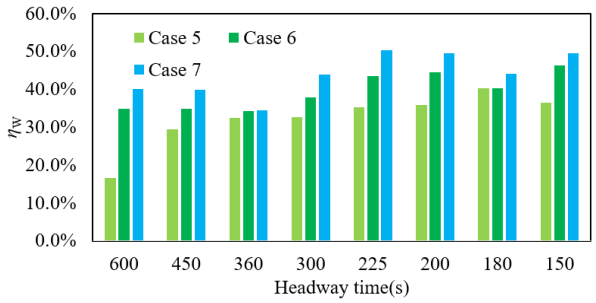

Fig. 24 The η_W of different headway times

It can be seen that the W_{TR} all increases with the decrease of the headway time. In Case 1, when the headway time decreases, η_W increases in the general trend, while the γ_{DCLoss} decreases in the general trend.

For Case 5, Case 6, and Case 7, the headway time of maximum η_W is 180s, 200s, and 225s, respectively. The headway time of maximum η_W in Case 5 and Case 7 is consistent with the headway time of the minimum γ_{DCLoss}, indicating that there is a close correlation between DC loss and system energy consumption.

Compared with Case 5, in Case 6 and Case 7, the r is smaller, and the γ_{DCLoss} is smaller. The W_{TR} decreases and η_W increases. In Case 7, compared with Case 5, γ_{DCLoss} is reduced by 13.4% at most, and η_W is increased by 23.5% at most.

E. Energy Correlation Analysis

To study what factors cause the change in electricity consumption, energy correlation analysis is necessary. The Pearson correlation coefficient is introduced. It is used to evaluate the correlation between two variables, as shown in (16), where cov (X, Y) is the covariance between variables X and Y. σ_X and σ_Y are the standard deviation of X and Y. The closer the Pearson correlation coefficient gets to 1, the higher the positive correlation of the two curves is [35]. If the coefficient is close to -1, it means X and Y

have a strong negative relationship. If the coefficient is close to 0, it means X and Y have a weak relationship or do not have a relationship.

$$\rho_{X,Y} = \frac{\mathrm{cov}(X,Y)}{\sigma_X \sigma_Y} \tag{16}$$

The Pearson coefficients between W_{TR} and other energies under different headway times are calculated. The results are shown in Table IX. It can be seen that the correlation coefficients between W_{ETT}, W_{DCLoss}, W_F, $W_{F\text{-}S}$, $W_{res,}$ and W_{TR} are high. To further explore the relationship between these energies and W_{TR}, the Pearson coefficients of different upward and downward departure time differences under each headway time are calculated.

TABLE IX PEARSON COEFFICIENTS BETWEEN WTR AND OTHER ENERGIES UNDER DIFFERENT HEADWAY TIMES

W_{ETT}	W_{DCLoss}	W_F	$W_{F\text{-}S}$	W_{res}
1.00	0.97	0.95	0.95	0.88

The Pearson coefficients between W_{TR} and other energy under different headway times are shown in Fig. 21. It can be seen that the positive correlation between W_{res} or W_{DCLoss} and W_{TR} is high. This phenomenon is consistent with the conclusion derived from (3).

When the headway time is 150s, the Pearson coefficient between W_{res} and W_{TR} is 0.12. It indicates that the difference between upward and downward departure time has little influence on W_{res}. The negative correlation between W_F and W_{TR} is the highest as 1, indicating that the RBE should be avoided feedback to EFS through reasonable control at this time.

When the headway time is 600s, the negative correlation between W_F or $W_{F\text{-}S}$ and W_{TR} is the highest. They are less than -0.7. The positive correlation between W_{ETT} and W_{TR} is the highest, which is 0.73. The feedback power of EFS should be increased as much as possible, and the feedback power should be absorbed by the step-down load as much as possible, while the ETT should be suppressed.

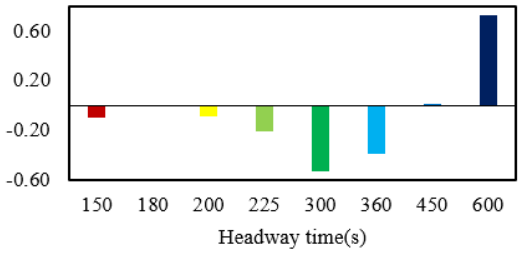

(a)

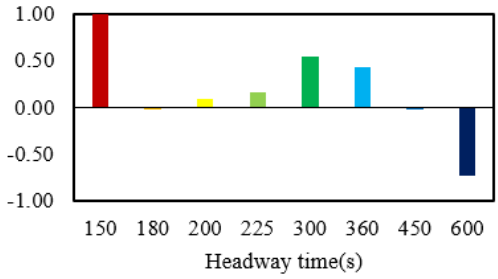

(b)

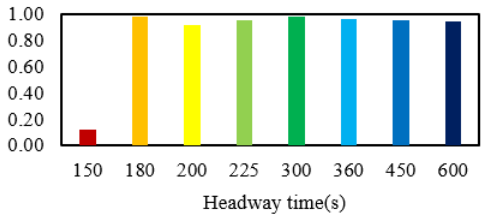

(c)

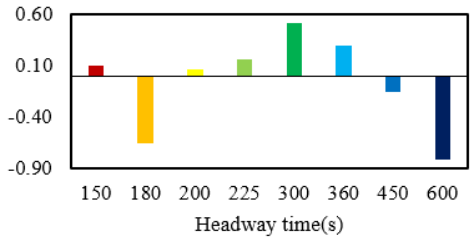

(d)

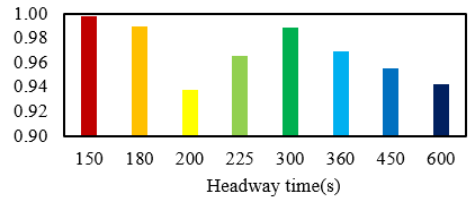

(e)

Fig. 21 The Pearson coefficients between W_M and other energy under different headway times (a)W_{ETT} (b) W_F (c) W_{res} (d) $W_{F\text{-}S}$ (e) W_{DCLoss}

In the operation of urban rail, W_{ETT} cannot be observed directly. From Fig. 11, it can be seen that the greater the distance of power transmission of ETT, the lower the efficiency. When adjusting the train running timetable, for the small headway time, the W_{ETT} can be increased by properly reducing the distance between the regenerative braking trains and the traction trains, to save energy consumption at the system level.

V. Conclusion

In this paper, RBE utilization is analyzed in different dimensions. The CF is defined. The improved iterative AC/DC power flow algorithm which considers the constant power state of EFS and on-board resistance is proposed. The main conclusions are:

1) The key to energy saving includes reducing the energy consumption of on-board resistance, the loss of DC TN, and the energy fed to MSs. In the CF process, the power loss on AC cables can be neglected compared with converter loss.

2) In the double-train static system, the long distance between trains is preferable to CF but adverse to efficient energy transfer. Turning off EFS will decrease the efficiency because the disappearance of CF increases the DC loss. To improve partial efficiency of operation, promoting CF when trains are far away from each other is a feasible method. In the multi-train dynamic system, with the increase of headway time, the RBE will gradually transfer from ETT to EFSs. The potential of promoting system efficiency by focusing on CF and energy fed to MSs is little.

3) Compared with the catenary and rail system, in the fourth-rail system, γ_{DCLoss} reduces by 13.4% at most and η_{W} increases by 23.5% at most. The TN resistance and DC Loss can influence the system energy utilizing efficiency greatly.

4) Reducing the energy consumption of on-board resistance, and the loss of DC TN can help the system energy saving. The correlation analysis can prove it. In operation, when the headway time is little, RBE should be avoided feedback to EFS through reasonable control, while feedback power of EFS should be advocated when the headway time is large.

Future research will focus on the optimization of the train timetable based on the results of this paper. The optimal objective may change due to the coefficient analysis in this paper. Reasonable control of EFSs is another research emphasis for higher system efficiency.

REFERENCES

[1] M. Khodaparastan, A. A. Mohamed and W. Brandauer, "Recuperation of Regenerative Braking Energy in Electric Rail Transit Systems," IEEE Transactions on Intelligent Transportation Systems, vol. 20, no. 8, pp. 2831-2847, Aug. 2019.

[2] T. Wu, W. Liu, J. Zhang, Y. Li, T. Li and B. He, "Analysis of Wayside Energy Storage System in DC Traction Power Supply System," 2019 IEEE Vehicle Power and Propulsion Conference (VPPC), Hanoi, Vietnam, 2019, pp. 1-6.

[3] J. Zhang, W. Liu, Z. Tian, H. Zhang, J. Zeng, and H. Qi. "Modelling, simulating and parameter designing for traction power system with bidirectional converter devices." IET Generation, Transmission & Distribution, vol. 16, no. 1, pp. 110-122, 2021.

[4] X. Shen, H. Wei and T. T. Lie, "Management and Utilization of Urban Rail Transit Regenerative Braking Energy Based on the Bypass DC Loop," IEEE Transactions on Transportation Electrification, vol. 7, no. 3, pp. 1699-1711, Sept. 2021.

[5] C. Wen, and K.Fang, "Control of Circulating Current for Direct-Parallel Connected PWM Inverters," Advanced Materials Research, vol. 756, pp. 612-617, 2013.

[6] S. Xu, W. Cao, K. Liu, S. Wang and J. Zhao, "Analysis and Control of Switching Circulating Currents in Multi-Module Parallel SPWM Converters," IEEE Access, vol. 6, pp. 32637-32648, 2018.

[7] PD CLC/TR 50646:2015.

[8] M. Dominguez, A. Fernández-Cardador, A. P. Cucala and R. R. Pecharroman, "Energy Savings in Metropolitan Railway Substations Through Regenerative Energy Recovery and Optimal Design of ATO Speed Profiles," IEEE Transactions on Automation Science and Engineering, vol. 9, no. 3, pp. 496-504, July 2012.

[9] K. Wang, H. Hu, J. Chen, J. Zhu, X. Zhong and Z. He, "System-Level Dynamic Energy Consumption Evaluation for High-Speed Railway," IEEE Transactions on Transportation Electrification, vol. 5, no. 3, pp. 745-757, Sept. 2019.

[10] X. Yang, X. Li, B. Ning and T. Tang, "A Survey on Energy-Efficient Train Operation for Urban Rail Transit," IEEE Transactions on Intelligent Transportation Systems, vol. 17, no. 1, pp. 2-13, Jan. 2016.

[11] Q. Qin, T. Guo, F. Lin and Z. Yang, "Energy Transfer Strategy for Urban Rail Transit Battery Energy Storage System to Reduce Peak Power of Traction Substation," IEEE Transactions on Vehicular Technology, vol. 68, no. 12, pp. 11714-11724, Dec. 2019.

[12] A. González-Gil, R. Palacin, P. Batty, and J. Powell, "A systems approach to reduce urban rail energy consumption." Energy Conversion and Management, vol. 80, pp. 509-524, 2014.

[13] González-Gil, A., R. Palacin, and P. Batty. "Optimal energy management of urban rail systems: Key performance indicators." Energy Conversion and Management, vol. 90, pp. 282-291, 2015.

[14] R. R. Pecharroman, A. Lopez-Lopez, A. P. Cucala and A. Fernandez-Cardador, "Riding the Rails to DC Power Efficiency: Energy efficiency in dc-electrified metropolitan railways.," IEEE Electrification Magazine, vol. 2, no. 3, pp. 32-38, Sept. 2014.

[15] Z. Tian, N. Zhao, S. Hillmansen, S. Su, and C. Wen. "Traction Power Substation Load Analysis with Various Train Operating Styles and Substation Fault Modes." Energies, vol. 13, no. 11, pp. 2788, 2020.

[16] Z. Tian, G. Zhang, N. Zhao, S. Hillmansen, P. Tricoli and C. Roberts, "Energy Evaluation for DC Railway Systems with Inverting Substations," 2018 IEEE International Conference on Electrical Systems for Aircraft, Railway, Ship Propulsion and Road Vehicles & International Transportation Electrification Conference (ESARS-ITEC), Nottingham, UK, 2018, pp. 1-6.

[17] B. Mohamed, P. Arboleya and C. González-Morán, "Modified Current Injection Method for Power Flow Analysis in Heavy-Meshed DC Railway Networks With Nonreversible Substations," IEEE Transactions on Vehicular Technology, vol. 66, no. 9, pp. 7688-7696, Sept. 2017.

[18] W. Liu, Q. Li and M. Chen, "Study of the simulation of DC traction power supply system based on AC/DC unified Newton-Raphson method," 2009 International Conference on Sustainable Power Generation and Supply, Nanjing, China, 2009, pp. 1-4.

[19] M. Z. Chymera, A. C. Renfrew, M. Barnes and J. Holden, "Modeling Electrified Transit Systems," IEEE Transactions on Vehicular Technology, vol. 59, no. 6, pp. 2748-2756, July 2010..

[20] P. Arboleya, B. Mohamed, C. González-Morán and I. El-Sayed, "BFS Algorithm for Voltage-Constrained Meshed DC Traction Networks With Nonsmooth Voltage-Dependent Loads and Generators," IEEE Transactions on Power Systems, vol. 31, no. 2, pp. 1526-1536, March 2016.

[21] P. Arboleya, B. Mohamed and I. El-Sayed, "DC Railway Simulation Including Controllable Power Electronic and Energy Storage Devices," IEEE Transactions on Power Systems, vol. 33, no. 5, pp. 5319-5329, Sept. 2018.

[22] P. Arboleya, G. Diaz and M. Coto, "Unified AC/DC Power Flow for Traction Systems: A New Concept," IEEE Transactions on Vehicular Technology, vol. 61, no. 6, pp. 2421-2430, July 2012.

[23] Lebre, José Rafael, Paulo Max Maciel Portugal, and Edson Hirokazu Watanabe. "Hybrid HVDC (H2VDC) system using current and voltage source converters," Energies vol. 11, no. 6, pp. 1323, 2018.

[24] W. Liu, Y. Lou, J. Zhang, X. Ye and R. Zhou. "Unified AC/DC Power Supply Calculation Taking into account Urban Rail Inverter Feedback Devices." Transactions of China Electrotechnical Society, vol. 34, no. 20, pp. 4381-4391, 2019.

[25] W. Liu, J. Zhang, H. Wang, T. Wu, Y. Lou and X. Ye, "Modified AC/DC Unified Power Flow and Energy-Saving Evaluation for Urban Rail Power Supply System With Energy Feedback Systems," IEEE Transactions on Vehicular Technology, vol. 70, no. 10, pp. 9898-9909, Oct. 2021.

[26] G. Zhang, Z. Tian, P. Tricoli, S. Hillmansen, Y. Wang and Z. Liu, "Inverter Operating Characteristics Optimization for DC Traction Power Supply Systems," IEEE Transactions on Vehicular Technology, vol. 68, no. 4, pp. 3400-3410, April 2019.

[27] Y. Huang, L. Yang, T. Tang, F. Cao and Z. Gao, "Saving Energy and Improving Service Quality: Bicriteria Train Scheduling in Urban Rail Transit Systems," IEEE Transactions on Intelligent Transportation Systems, vol. 17, no. 12, pp. 3364-3379, Dec. 2016.

[28] Liu, J.; Zhao, N. Research on Energy-Saving Operation Strategy for Multiple Trains on the Urban Subway Line. Energies 2017, 10(12), 2156

[29] P. Wang, R. Goverde, Multi-train trajectory optimization for energy efficiency and delay recovery on single-track railway lines, Transportation Research Part B: Methodological, Vol. 105, pp. 340-361, 2017

[30] I. E. Demirci and H. B. Celikoglu, "Timetable Optimization for Utilization of Regenerative Braking Energy: A Single Line Case over Istanbul Metro Network," 2018 21st International Conference on Intelligent Transportation Systems (ITSC), Maui, HI, USA, 2018, pp. 2309-2314.

[31] Ning, Jingjie, Yonghua Zhou, Fengchu Long, and Xin Tao. "A synergistic energy-efficient planning approach for urban rail transit operations," Energy vol. 151, pp. 854-863, 2018.

[32] Z. Pan, M. Chen, S. Lu, Z. Tian and Y. Liu, "Integrated Timetable Optimization for Minimum Total Energy Consumption of an AC Railway System," in IEEE Transactions on Vehicular Technology, vol. 69, no. 4, pp. 3641-3653, April 2020.

[33] M. Shang, Y. Zhou and H. Fujita, "Energy-Saving Operation Synergy for Multiple Metro-Trains Using Map-Reduce Parallel Optimization," IEEE Transactions on Vehicular Technology, vol. 71, no. 2, pp. 1319-1332, Feb. 2022.

[34] J. Zhang, Jian, W. Liu, Z. Tian, H. Qi, J. Zeng, and Y. Yang, "Urban rail substation parameter optimization by energy audit and modified salp swarm algorithm", IEEE Transations on Power Delivery, vol. 37, no. 6, pp. 4968-4978, Dec. 2022.

[35] L. Sheugh and S. H. Alizadeh, "A note on pearson correlation coefficient as a metric of similarity in recommender system," 2015 AI & Robotics (IRANOPEN), Qazvin, Iran, 2015, pp. 1-6.